Observation of higher-order contribution to anisotropic magnetoresistance of thin Pt/[Co/Pt] multilayered films

Wen-Bin Wu[1], Julia Kasiuk[2], Janusz Przewoźnik[3], Czesław Kapusta[3], Ivan Svito[2], Dang Thanh Tran[4], Hung Manh Do[4], Hung Manh Dinh[5], Johan Åkerman[6], Thi Ngoc Anh Nguyen[4,7,*]

[1]College of Physical Science and Technology, Dalian University, Dalian 116622, China

[2]Faculty of Physics, Belarusian State University, 4 Nezavisimosti ave., Minsk 220030, Belarus

[3]AGH University of Krakow, Faculty of Physics and Applied Computer Science, Department of Solid State Physics, Krakow 30-059, Poland

[4]Institute of Materials Science, Vietnam Academy of Science and Technology, 18 Hoang Quoc Viet, Cau Giay, Hanoi 11355, Vietnam

[5]Physics Department, Hanoi National University of Education, 144 Xuan Thuy, Cau Giay, Hanoi, Vietnam

[6]Department of Physics, University of Gothenburg, Göteborg 41296, Sweden

[7]Graduate University of Science and Technology, Vietnam Academy of Science and Technology, 18 Hoang Quoc Viet, Cau Giay, Hanoi 11355, Vietnam

*ngocanhnt.vn@gmail.com

Abstract

We studied the magnetoresistance mechanisms in a Pt/$[Co/Pt]_{x5}$ film consisting of a ferromagnetic $[Co/Pt]_{x5}$ layer with strong perpendicular magnetic anisotropy and a nonmagnetic Pt layer with strong spin-orbit coupling. We revealed two competing contributions of the $\sin^2\theta$ and $\cos^4\theta$ types to its angular and magnetic field dependences of electrical resistance at T = 10-250 K corresponding to the out-of-plane rotation of the magnetization $M(\theta)$ perpendicularly to the electric current. They were attributed to different magnetoresistance mechanisms. The higher-order $\cos^4\theta$ contribution, which emerges and increases with decreasing temperature, is attributed to the anisotropic magnetoresistance of the ferromagnetic layer, while the $\sin^2\theta$ contribution, which prevails at room temperature and then decreases, is mainly associated with the spin Hall magnetoresistance originating from the Pt layer. The analysis of the corresponding angular dependences of the Hall voltage revealed non-trivial periodic oscillations in the second harmonic. Their appearance is found to be consistent with the manifestation of higher-order angle-dependent contributions to the field-like spin-orbit torque. The revealed strong influence of the electric current on the magnetization of the film studied, which ensures the higher-order effects manifestation, is of high relevance for magnetic memory design technologies.

Keywords: multilayered films, perpendicular magnetic anisotropy, anisotropic magnetoresistance, spin Hall magnetoresistance, magnetic proximity, spin-orbit torque

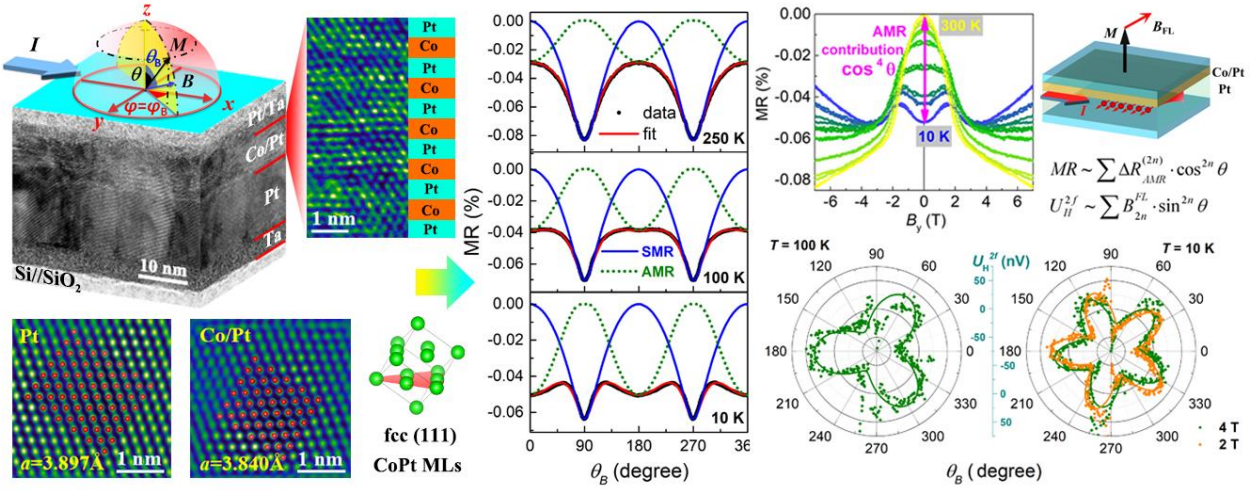

1. Introduction

A possibility of mutual conversion between two intrinsic properties of an electron, *i.e.* its charge and spin, by means of spin-orbit coupling (SOC) is of undoubted practical importance for spintronics and is one of the leading directions of relevant scientific research. The coupling between spin and orbital motion of an electron, which is capable of generating a pure spin current in a conductor with charge current and the accumulation of spins at its surfaces (interfaces), has been intensively studied over the past decades for different materials and their combinations [1-16]. In bilayers consisting of a nonmagnetic heavy metal (HM) with strong SOC and a ferromagnet (F), a spin accumulation at the HM/F interface via the mechanisms known as spin Hall effect (SHE) and Rashba-Edelstein effect can exert a torque on the magnetic moments of the ferromagnetic layer leading to their precession or even complete reversal [2, 9, 11, 12, 17]. This finding, namely, the spin-orbit torques (SOTs) induced magnetization switching, has revolutionized the approaches to the design of magnetic memory [4, 6, 18, 19], replacing the mechanism of spin transfer from a ferromagnetic polarizer to a free ferromagnetic layer. Therefore, the search for novel materials with a strong SOC and the design of multilayered compositions with advanced interface architecture to enhance the SOT efficiency [16] are the challenges of a high relevance.

Two different mechanisms are typically considered for describing the source of spin accumulation at the HM/F interface, namely, a bulk-type SHE generating spin current in the bulk of 5*d* (Pt, Ir, Ta, W, Hf) or 4*d* (Pd) HM layer and an interfacial-type Rashba effect generating interfacial spin accumulation in the systems with broken inversion symmetry due to the strong SOC of carriers [1, 3, 9, 20, 21]. Since both mechanisms demonstrate the same symmetry, regardless the effect, they both can contribute in a similar way to the exerted SOTs, transverse (or field-like torque T_{FL}) and longitudinal (or damping-like torque T_{DL}), which affect the magnetic moments of ferromagnetic layer [2, 20]. A commonly used method for detecting SOTs action on the magnetization, as well as for estimating their efficiency, is to measure the Hall voltage at the alternating current (*ac*) harmonics [2, 22-24]. The current-induced magnetization oscillations modulate the Hall voltage, while the corresponding changes are detected in the second harmonic component.

Another elegant way to evaluate the T_{DL} efficiency (spin Hall angle) in the HM/F bilayers involves the measurements of angular dependences of their magnetoresistance (MR), with the current-induced changes being detectable even in a dc current mode [11, 24-27]. Such changes, referred to as the spin Hall MR (SMR), are established to arise due to the asymmetry in the absorption and reflection of the spin current generated by the bulk SHE of the HM upon rotation of the magnetization of an adjacent ferromagnet [3]. However, the SMR turned out to be the

most debatable mechanism. Initially, it was proposed and successfully applied for interpreting the angle-dependent MR of the HM/FI bilayers, where FI is a ferromagnetic insulator [27-29]. However, in the HM/FM bilayers, where FM is a ferromagnetic metal, which are more relevant for applications, additional MR mechanisms with similar manifestation (symmetry) can contribute due to charge current passing through the FM, like anisotropic MR (AMR) and anisotropic interface MR (AIMR). They arise due to the influence of SOC on the scattering of electrons in the bulk FM and at its interface(s) [3, 30, 31]. Therefore, despite the fact that the SMR contribution to MR of the HM/FM bilayers has been reliably proven [32-36], the SOT efficiency estimated in this way can be erroneous [25], since it is difficult to separate out a pure SMR effect [24].

In spite of the various developed approaches to adapt and extend the theory describing the SMR mechanism to all-metallic bilayers and multilayers (MLs) [32-40], heated debate about the origin of the observed MR effects has not subsided for a decade. In general, the SMR mechanism can be distinguished from the AMR one, which is a fundamental magneto-transport property of FMs, by their different angular dependences, since the out-of-plane rotation of magnetization perpendicular to the current changes the resistance according to the SMR mechanism, but does not change it according to the AMR mechanism. However, a series of works devoted to the detailed study of AMR in thin FM layers [30, 31, 41] have verified that the assumption of a constant AMR effect in the plane perpendicular to the current is not valid for textured and layered films due to the symmetry reasons. The impact of crystallinity and interface-scattering anisotropy should be considered in such systems, which can provide additional contributions to AMR that depend on the polar angle θ of the out-of-plane magnetization rotation. This makes the SMR and AMR mechanisms indistinguishable due to their similar angular dependence of the $\cos^2\theta$-type [3]. The proposed approaches of extracting pure SMR/AMR effects are mainly based on verifying the dependences of the observed MR effect on the thickness of each layer, HM and FM, [31, 33, 42, 43] and on comparing the estimated spin Hall angle with that obtained by other methods [11, 24, 25, 43]. However, there is still no absolute agreement in the results of the above studies, as well as in the unambiguous interpretation of the MR mechanisms in HM/FM bilayers [3, 41].

The present work is focused on the low-temperature study (T = 10-250 K) of the angular and magnetic field dependences of MR in a Pt/[Co/Pt] bilayer, which contains [Co/Pt] MLs as an FM layer with very strong perpendicular magnetic anisotropy (PMA) (anisotropy field B_A of 2 T) and Pt as a HM layer with strong SOC, to verify its MR mechanisms. Although the ordinary and widely studied materials are chosen for the layers, our film demonstrates atypical and intriguing dependences of MR on both the magnitude and orientation of the applied magnetic field, which

indicate the contribution of several effects with different physical mechanisms standing behind them. Their interpretation made it possible to distinguish both the SMR and AMR contributions to the electron transport in the film studied. A higher-order term of $\cos^4\theta$-type is shown to appear with decreasing temperature, which was predicted for such films from symmetry considerations [41], but has never been experimentally observed in Pt/Co systems before. The interpretation of the low-temperature peculiarities of MR takes into account the influence of a magnetic proximity effect (MPE) in Pt. Additionally, the results of Hall voltage analysis in the second harmonic are presented, where non-trivial angular dependences, demonstrating periodic oscillations, are revealed. Their appearance is found to be consistent with the manifestation of anisotropic contributions to the T_{FL} SOT [2, 3, 44].

2. Experimental

The Pt/[Co/Pt] thin film with nominal composition of $Ta_{5\ nm}/Pt_{15\ nm}/[Co_{0.4\ nm}/Pt_{0.8\ nm}]_{x5}/Pt_{3\ nm}/Ta_{5\ nm}$ (from bottom to top) was deposited on thermally oxidized flat Si wafers using ultra-high vacuum magnetron sputtering system (AJA International, Inc., USA) with a base pressure lower than 4×10^{-6} Pa. During film deposition, the working pressure was 0.67 Pa under a fixed Ar flow rate of 25 sccm. The top Ta layer was used as a capping layer to prevent oxidation of the MLs, while the thick bottom Ta/Pt bilayer serves to promote strong (111) texture and to improve the perpendicular anisotropy of the subsequent [Co/Pt] MLs. The layer thicknesses were determined from the deposition time and calibrated deposition rates.

Microstructural studies have been performed with a high resolution transmission electron microscopy (HRTEM) using FEI Tecnai G2 F20 X-Twin microscope, which operates at 200 kV. The samples were prepared for cross-sectional analysis by focused ion beam (FIB) technique using a dual beam FEI Strata 400S microscope. The data were analyzed with Gatan DigitalMicrograph GMS 3 and VESTA software.

The structures and phase compositions of the deposited Pt/[Co/Pt] film were examined by X-ray diffraction (XRD) using an Empyrean PANalytical diffractometer with Cu K_α radiation (λ = 0.15418 nm). The experimental data were collected at room temperature (RT) in the conventional Bragg-Brentano theta-theta geometry, with the diffraction angle 2Θ between the incident beam and detector being scanned in the range of 10º-130º. The experimental data were analyzed using HighScore Plus software and fitted with the FullProf program [45] based on the Rietveld method.

The magnetic properties of the Pt/[Co/Pt] film were characterized using the vibrating sample magnetometry (VSM) option of the Quantum Design Physical Property Measurement

System (PPMS) in the temperature range T = 3-300 K. A magnetic field with induction B up to 9 T was applied along the film normal and in the film plane. The linear diamagnetic contribution from the substrate was subtracted from the raw experimental field dependences of magnetization.

The magnetotransport properties of the Pt/[Co/Pt] film were measured at T = 3-300 K by a standard four-probe method using the *direct current (dc) resistivity* and *alternating current (ac) transport* options of PPMS, equipped with a rotating sample holder. A *dc* current I of 5 mA or an *ac* current with the frequency of 103 Hz and amplitude I_0 of 4 mA was applied using current-carrying contacts (I), and the value of electrical potential difference was measured using voltage-sensing contacts placed in-line with current-carrying contacts (U) and perpendicular to them (U_H), as shown in the scheme of electrical contacts arrangement in Fig. 1. The longitudinal resistance R was calculated as $R = U/I$. In the *ac* mode, the harmonic Hall-voltage measurements were performed by taking the Fourier transform of the Hall voltage, with the signal being decomposed into the first harmonic (U_H^f) and second harmonic (U_H^{2f}) components.

The R and U_H were measured depending on the direction and magnitude of the applied magnetic field B. The field dependences $R(B)$ and $U_H(B)$ were measured in B field swept in the range of -9 – +9 T in two orthogonal directions, perpendicular to the film plane (along z axis) and in the film plane, but perpendicular to the electric current (along y axis), as shown in Fig. 1. The angular dependences $R(\theta_B)$ and $U_H(\theta_B)$ were measured in the constant-value field B rotating in zy plane (perpendicular to the electric current) in the angle range θ_B = 0-360° (step $\Delta\theta_B$ = 1°) counted from the film normal (Fig. 1). For signal processing, the averaging over two permutations of the pair of voltage-sensing contacts (both, for longitudinal or transverse pair) was carried out to eliminate a possible parasitic signal from the contacts with opposite parity, which may occur due to the asymmetry of the voltage probes and spread in current directions.

3. Results and discussion

3.1. Structure and phase composition

XRD pattern of the Pt/[Co/Pt] film is shown in Fig. 2(a). The intense peak at 2Θ = 40.04º, corresponding to the face-centered cubic (*fcc*) lattice with a cell parameter a = 3.899 Å close to that characterizing the Pt bulk phase (a = 3.911 Å [46, 47]), dominates in the pattern and overlaps the rest of the peaks. It relates to the thick 15-nm Pt underlayer (or buffer layer). A distinct (111)-texture is characteristic of the Pt underlayer, and no detectable peaks corresponding to other crystal orientations are found…

3.2. Magnetic anisotropy

Magnetization curves of the Pt/[Co/Pt] film, which are measured directly by VSM and estimated from the anomalous Hall effect (AHE) voltage U_{AHE} in two perpendicular-to-current directions of the external magnetic field B, i.e. along the film normal (B_z) and in the film plane (B_y), are shown in Fig. 3. The data are presented as m_z and m_z projections of magnetization M on the corresponding axes normalized to the saturation value M_S of each curve. Color gradient shows the gradual temperature change in the range T = 3-100 K. The evolution of m_z projection of magnetization in the field B sweeping in z direction (Fig. 3(a)) can be equally estimated from both the magnetometry $M(B_z)$ and Hall-voltage $U_{AHE}(B_z)$ curves, with the similar field dependences being obtained. Inversely, the in-plane $U_{AHE}(B_y)$ and $M(B_y)$ curves (Figs. 3(b) and 3(c)) provide correspondingly the $m_z(B_y)$ and $m_y(B_y)$ dependences. The curves shown in Fig. 3(a) are extracted from the raw Hall voltage signal $U_H(B_z)$ by removing the contribution of an ordinary Hall voltage and considering that $U_{AHE}(B) = I \cdot \Delta R_{AHE} \cdot m_z(B)$ for perpendicular-to-current magnetization rotation ($\varphi = \varphi_B = 90°$), where ΔR_{AHE} is the coefficient of AHE. Small out-of-plane field tilting of 5º from y axis is introduced for achieving coherent magnetization rotation in Fig. 3(b)…

3.3. Magnetoresistance

3.3.1. Angular dependences of magnetoresistance

The angular dependences of electrical resistance $R(\theta_B)$ of the studied Pt/[Co/Pt] film in the external magnetic field B = 4 T rotating in zy plane are shown in Fig. 4(a) for different temperatures T = 250 K, 100 K and 10 K. The experimental curves are normalized to the amplitude of the resistance change at each temperature, *i.e.* $\Delta R(\theta_B)/\Delta R_{max} = (R(\theta_B)-R_{min})/(R_{max}-R_{min})$. The applied field of 4 T exceeds significantly the anisotropy field B_A ~ 1.6-2 T of the film in the whole inspected temperature range (Fig. 3(c)) and is supposed to be sufficient to completely saturate the film magnetization.

The shape of the $\Delta R(\theta_B)$ curve at T = 250 K (Fig. 4(a)) looks consistent with that for the SMR effect characteristic of HM/FM bilayers [3, 11, 26, 38, 58], which provides the angular dependence of resistance $R(\theta_B)$ according to

$$R(\theta) = R_0 - \Delta R_{SMR} \cdot sin^2\theta \quad (1)$$

in the case of M rotation in zy plane, i.e. for $\varphi = 90°$, where the resistance R is typically independent of AMR effect. Here, R_0 is the isotropic contribution to the longitudinal resistance independent of the magnetization orientation, ΔR_{SMR} is the amplitude of the SMR effect, and θ is a polar angle of M orientation in spherical coordinates (Fig. 1). The clear minima of the R value at $\theta_B = 90°$ and 270° correspond to the alignment of the FM magnetization parallel to the spin

polarization σ in Pt at the Pt/FM interface [59]. Here we do not consider effects that provide a linear change in *R* with applied current, such as unidirectional SMR (USMR) [58], which implies different resistance for parallel and antiparallel orientation of *M* and σ. This effect is negligible in Pt/Co systems at such low current densities as those used in this study (~10^5 A/cm^2), and therefore can be neglected when averaging over two opposite current directions…

3.3.2. Field dependences of magnetoresistance

The anomalies in the low-temperature MR of the studied Pt/[Co/Pt] film are also revealed in its field dependences of electrical resistance $R(B)$. As shown in Fig. 5(a), at higher temperatures (e.g. at T = 200 K), the shape of $R(B_z)$ and $R(B_y)$ curves satisfies the SMR mechanism expected for similar Co/Pt bilayers [11, 25, 32, 38]. Namely, besides a conventional Lorentz MR mechanism providing B^2 isotropic dependence of $R(B)$ in high fields, a negative contribution to the *R* signal appears in the $R(B_y)$ curve as a decrease in the resistance in $B \leq B_A$ due to the FM magnetization rotation towards the *y* axis, which is parallel to the Pt polarization σ…

3.3.3. Mechanisms

The approximations shown in Fig. 4(d) and 5(c) perfectly match the experimental $R(\theta_B)$ and $R(B)$ curves, with the competition between the two contributing $\sin^2\theta$ and $\cos^4\theta$ components being evident. A similar ~$\cos^4\theta$ contribution to the angular dependences of MR was previously detected for the Pt/Ni/Pt sandwiches and associated with the AMR mechanism arising due to the film crystalline texture [41]. Despite the fact that the conventional AMR mechanism declares simple $\cos^2\psi$ dependence of the resistance on the orientation of the FM magnetization ψ with respect to the current, this is inapplicable for structurally anisotropic films. Taking into account the symmetry arising from the *fcc* (111) texture and layered structure of thin films, a relation for the AMR can be obtained in the form of a series $\sum \Delta R_{2n} \cdot cos^{2n}\theta$, which implies its explicit dependence on the polar angle θ of magnetization even for *M* rotation in the plane perpendicular to the current direction (φ = 90°) [41-43]. Each term ΔR_{2n} in the series potentially consists of the bulk and interfacial contributions due to the *fcc* (111) texture and uniaxial anisotropy of the interfaces, respectively. Thus, the second-order term ΔR_2 was attributed to the contributions of bulk geometrical size effect (GSE) and interfacial AIMR effect. The fourth-order term ΔR_4 typically includes only bulk-type contribution, while the interface-scattering anisotropy of the fourth order is zero within the error margins [41]. The higher-order terms with $2n \geq 6$ are typically omitted due to their small ΔR_{2n} amplitude, but can contribute significantly at low temperatures [41]…

3.4. Second harmonic Hall voltage

Analysis of *ac* Hall voltage of the studied Pt/[Co/Pt] film revealed a detectable U_H^{2f} signal in the second harmonic both in the field and scanning modes (Fig. 6), i.e. for the external field *B* sweeping along *y* axis or rotating in *zy* plane, respectively. The shape of $U_H^{2f}(B_y)$ curve (Fig. 6(a)) looks similar to that for the AlO_x/Co/Pt and MgO/CoFeB/Ta trilayers, for which the detected signal has been associated with the action of current-induced SOTs provided by bulk SHE and/or interfacial Rashba effect on magnetization orientation [2, 7, 11, 22, 44, 52, 65].

In contrast to this, the angular dependences $U_H^{2f}(\theta_B)$ of the studied Pt/[Co/Pt] film shown in Fig. 6(c)-(h) demonstrate distinct sinusoidal oscillations of voltage, which have not been reported for similar bi- or multi-layers. Interestingly, the period of oscillations changes with temperature from $5\cdot\theta_B$ at 10 K (Fig. 6(c)) to $3\cdot\theta_B$ (Fig. 6(d)) at 100 K, with no periodic oscillations being detectable at $T = 250$ K. It should be mentioned that we do not expect the contribution of the thermoelectric effects, associated mainly with the anomalous Nernst effect (ANE), induced by Joule heating, since moderate current densities less than 10^5 A/cm^2 are applied in the present study. In addition, the thermoelectric transverse voltage contribution was previously shown to be negligibly small in Pt/Co layers [58, 65, 66], with the angular dependence of another type (~cos(θ)) being characteristic of the ANE in the second harmonic voltage [7]...

4. Conclusions

A low-temperature study of MR and Hall voltage was carried out for the thin Pt/[Co/Pt] multilayered film containing the [Co/Pt] MLs, which serve as an FM layer with a strong PMA ($B_A \sim 2$ T), in contact with the Pt HM layer with high SHE. A strong bulk and interfacial SOC provides intricate combinations of quite different effects in the longitudinal MR and second harmonic Hall voltage, which can be specified and discriminated at low temperatures. In particular, the competition between the mechanisms of SMR in the HM layer and AMR in the FM layer provides a complex shape of the perpendicular-to-current angular dependences of MR, with the AMR contribution appearing as a fourth-order term of $\cos^4\theta$-type. Rarely observed higher-order contributions to AMR arise as a result of the anomalous manifestation of AMR effect in polar rotational geometry ($\varphi = 90°$) in the [Co/Pt] MLs with a pronounced *fcc* (111) texture and/or distinct layered structure of the [Co/Pt] MLs. The increase in the Pt polarization with decreasing temperature is found to be responsible for detecting a weak signal from the higher-order terms of MR in the studied film ($T \leq 100$ K), since it changes the balance between the second- and fourth-order contributions, suppressing the SMR and enhancing the AMR due to induced ferromagnetism.

The action of current-induced field-like SOT on the FM magnetization is revealed from the analysis of the second harmonic component of the *ac* Hall voltage, which shows detectable U_H^{2f} signal in the field and angular scans despite a rather low applied current density of 10^5 A/cm^2. A specific shape of the angular dependences $U_H^{2f}(\theta_B)$, which demonstrates periodic cosine oscillations, is revealed for the studied film at T = 10-100 K, with their period reducing with decreasing temperature. Such oscillations, which have not been previously reported for similar films, are associated with a low-temperature increase in the impact of higher-order angle-dependent terms $B_{2n}^{FL} \cdot sin^{2n}\theta$ ($2n$ = 2, 4…) contributing to the field-like SOT. The correlation is supposed to exist between the detected higher-order terms $\sum \Delta R_{AMR}^{(2n)} \cdot cos^{2n}\theta$ and $\sum B_{2n}^{FL} \cdot sin^{2n}\theta$ contributing to the low-temperature $R(\theta_B)$ and $U_H^{2f}(\theta_B)$ dependences, respectively. Both the anisotropic SOTs and MR contributions observed are expected to arise due to the anisotropic spin-dependent scattering at the HM/FM interface with strong SOC or inside the FM layer with pronounced uniaxial anisotropy caused by crystalline texture. The revealed correlation contributes to the insight into the SOTs-generation mechanisms, while the observed robust influence of the field-like SOT on the FM magnetization at the Pt/Co interface is promising for designing an electrically controlled magnetic memory and spin logic cells. The manifestation of anisotropic components of SOT indicates the high sensitivity of magnetization of the [Co/Pt] MLs to the injected electric current that opens up opportunities for implementing efficient SOT-induced magnetization switching in Pt/[Co/Pt] bilayers and their application as SOT-HM/FM junction in the next generation spin logic and memory devices.

Acknowledgement

This work was financially supported by Vietnam Academy of Science and Technology (VAST) under Project NCXS01.04/22-24.

References

[1] A. Hoffmann, Spin Hall Effects in Metals, IEEE Trans. Magn. 49 (2013) 5172. http://doi.org/10.1109/TMAG.2013.2262947.

[2] K. Garello, I.M. Miron, C.O. Avci, F. Freimuth, Y. Mokrousov, S. Blügel, S. Auffret, O. Boulle, G. Gaudin, P. Gambardella, Symmetry and magnitude of spin–orbit torques in ferromagnetic heterostructures, Nature Nanotech. 8 (2013) 587–593. https://doi.org/10.1038/nnano.2013.145.

[3] C.O. Avci, G. S. D. Beach, P. Gambardella, Effects of transition metal spacers on spin-orbit torques, spin Hall magnetoresistance, and magnetic anisotropy of Pt/Co bilayers, Phys. Rev. B 100 (2019) 235454. http://doi.org/10.1103/PhysRevB.100.235454.

[4] C. Engel, S. Goolaup, F. Luo, W. Gan, W.S. Lew, Spin-orbit torque induced magnetization anisotropy modulation in Pt/(Co/Ni)4/Co/IrMn heterostructure, J. Appl. Phys. 121 (2017) 143902. http://doi.org/10.1063/1.4980108.

[5] A. Ghosh, K. Garello, C.O. Avci, M. Gabureac, P. Gambardella, Interface-Enhanced Spin-Orbit Torques and Current-Induced Magnetization Switching of Pd/Co/AlO_x Layers, Phys. Rev. Appl. 7 (2017) 014004. http://doi.org/10.1103/PhysRevApplied.7.014004.
[6] Q. Shao *et al*., Roadmap of spin-orbit torques, IEEE Trans. Magn. 57 (2021) 800439. http://dx.doi.org/10.1109/TMAG.2021.3078583.
[7] X. Qiu, P. Deorani, K. Narayanapillai, K.-S. Lee, K.-J. Lee, H.-W. Lee, H Yang, Angular and temperature dependence of current induced spin-orbit effective fields in Ta/CoFeB/MgO nanowires, Sci. Rep. 4 (2014) 4491. http://doi.org/10.1038/srep04491
[8] M.-H. Nguyen, C.-F. Pai, K.X. Nguyen, D.A. Muller, D.C. Ralph, R.A. Buhrman, Enhancement of the anti-damping spin torque efficacy of platinum by interface modification, Appl. Phys. Lett. 106 (2015) 222402. http://dx.doi.org/10.1063/1.4922084
[9] I. M. Miron, G. Gaudin, S. Auffret, B. Rodmacq, A. Schuhl, S. Pizzini, J. Vogel, P. Gambardella, Current-driven spin torque induced by the Rashba effect in a ferromagnetic metal layer, Nature Mater. 9 (2010) 230-234. https://doi.org/10.1038/nmat2613
[10] A. Manchon, J. Železný, I.M. Miron, T. Jungwirth, J. Sinova, A. Thiaville, K. Garello, P. Gambardella, Current-induced spin-orbit torques in ferromagnetic and antiferromagnetic systems, Rev. Mod. Phys. 91 (2019) 035004. http://doi.org/10.1103/RevModPhys.91.035004.
[11] Y.-C. Lau, D. Betto, K. Rode, J.M.D. Coey, P. Stamenov, Spin–orbit torque switching without an external field using interlayer exchange coupling, Nature Nanotech. 11 (2016) 758–762. https://doi.org/10.1038/nnano.2016.84.
[12] W.-Y. Kwak, J.-H. Kwon, P. Grünberg, S. H. Han, B.K. Cho, Current-induced magnetic switching with spin-orbit torque in an interlayer-coupled junction with a Ta spacer layer, Sci. Rep. 8 (2018) 3826. http://doi.org/10.1038/s41598-018-22122-1.
[13] Z. Wang *et al*. Modulation of field-like spin orbit torque in heavy metal / ferromagnet heterostructure, Nanoscale 12 (2020) 15246-15251. http://doi.org/10.1039/D0NR02762F.
[14] Y. Kim, W. Jeong, D. Yun, G.-E. Ahn, O. Lee, Spin and orbital properties of perpendicular magnetic anisotropy for spin-orbit torque material devices, Appl. Surf. Science 544 (2021) 148959. https://doi.org/10.1016/j.apsusc.2021.148959.
[15] H. Chen, D. Yi, Spin‑charge conversion in transition metal oxides, APL Mater. 9 (2021) 060908. http://doi.org/10.1063/5.0052304.
[16] X. Qiu, W. Legrand, P. He, Y. Wu, J. Yu, R. Ramaswamy, A. Manchon, H. Yang, Enhanced Spin-Orbit Torque via Modulation of Spin Current Absorption, Phys. Rev. Lett. 117 (2016) 217206. http://doi.org/10.1103/PhysRevLett.117.217206.
[17] I.M. Miron, K. Garello, G. Gaudi, P.-J. Zermatten, M.V. Costache, S. Auffret, S. Bandiera, B. Rodmacq, A. Schuhl, P. Gambardella, Perpendicular switching of a single ferromagnetic layer induced by in-plane current injection, Nature 189 (2011) 476. http://doi.org/10.1038/nature10309.
[18] Y. Kim, X. Fong, K.-W. Kwon, M.-C. Chen, K. Roy, Multilevel Spin-Orbit Torque MRAMs, IEEE Transactions on Electron Devices 62 (2015) 561-568. http://doi.org/10.1109/TED.2014.2377721.
[19] H. Honjo *et al*., First demonstration of field-free SOT-MRAM with 0.35 ns write speed and 70 thermal stability under 400°C thermal tolerance by canted SOT structure and its advanced patterning/SOT channel technology, in *Proceedings of the International Electron Devices Meeting (IEDM), San Francisco, 2019* (IEEE, 2019), pp. 28.5.1-28.5.4. http://doi.org/10.1109/IEDM19573.2019.8993443.
[20] D.A. Pesin, A.H. MacDonald, Quantum kinetic theory of current-induced torques in Rashba ferromagnets, Phys. Rev. B 86 (2012) 014416. http://doi.org/10.1103/PhysRevB.86.014416.
[21] J. Kim *et al.*, Layer thickness dependence of the current-induced effective field vector in Ta|CoFeB|MgO, Nature Mater. 12 (2013) 240–245. https://doi.org/10.1038/nmat3522.
[22] C.O. Avci *et al*., Fieldlike and antidamping spin-orbit torques in as-grown and annealed Ta/CoFeB/MgO layers, Phys. Rev. B 89 (2014) 214419. http://doi.org/10.1103/PhysRevB.89.214419.

[23] M. Hayashi, J. Kim, M. Yamanouchi, H. Ohno, Quantitative characterization of the spin-orbit torque using harmonic Hall voltage measurements, Phys. Rev. B 89 (2014) 144425. http://doi.org/10.1103/PhysRevB.89.144425.
[24] M.-H. Nguyen, C.-F. Pai, Spin-orbit torque characterization in a nutshell, APL Mater. 9 (2021) 030902. http://doi.org/10.1063/5.0041123.
[25] Y.-C. Lau, M. Hayashi, Spin torque efficiency of Ta, W, and Pt in metallic bilayers evaluated by harmonic Hall and spin Hall magnetoresistance measurements, Japan. J. Appl. Phys. 56 (2017) 0802B5. https://doi.org/10.7567/JJAP.56.0802B5.
[26] S. Cho, S.C. Baek, K.-D. Lee, Y. Jo, B.-G. Park, Large spin Hall magnetoresistance and its correlation to the spin-orbit torque in W/CoFeB/MgO structures, Sci. Rep. 5 (2015) 14668. https://doi.org/10.1038/srep14668.
[27] Y.-T. Chen, S. Takahashi, H. Nakayama, M. Althammer, S.T.B. Goennenwein, E. Saitoh, G.E.W. Bauer, Theory of spin Hall magnetoresistance (SMR) and related phenomena, J. Phys.: Condens. Matter 28 (2016) 103004. http://dx.doi.org/10.1088/0953-8984/28/10/103004.
[28] M. Althammer *et al*., Quantitative study of the spin Hall magnetoresistance in ferromagnetic insulator/normal metal hybrids, Phys. Rev. B 87 (2013) 224401. https://doi.org/10.1103/PhysRevB.87.224401.
[29] H. Nakayama *et al.*, Spin Hall Magnetoresistance Induced by a Nonequilibrium Proximity Effect, Phys. Rev. Lett. 110 (2013) 206601. https://doi.org/10.1103/PhysRevLett.110.206601.
[30] A. Kobs, S. Heße, W. Kreuzpaintner, G. Winkler, D. Lott, P. Weinberger, A. Schreyer, and H.P. Oepen, Anisotropic Interface Magnetoresistance in Pt/Co/Pt Sandwiches, Phys. Rev. Lettt. 106 (2011) 217207. https://doi.org/10.1103/PhysRevLett.106.217207.
[31] A. Kobs, H.P. Oepen, Disentangling interface and bulk contributions to the anisotropic magnetoresistance in Pt/Co/Pt sandwiches, Phys. Rev. B 93 (2016) 014426. https://doi.org/10.1103/PhysRevB.93.014426.
[32] J. Kim, P. Sheng, S. Takahashi, S. Mitani, M. Hayashi, Spin Hall Magnetoresistance in Metallic Bilayers, Phys. Rev. Lett. 116 (2016) 097201. https://doi.org/10.1103/PhysRevLett.116.097201.
[33] M. Kawaguchi, D. Towa, Y.-C. Lau, S. Takahashi, M. Hayashi, Anomalous spin Hall magnetoresistance in Pt/Co bilayers, Appl. Phys. Lett. 112 (2018) 202405. https://doi.org/10.1063/1.5021510.
[34] Ł. Karwacki, K. Grochot, S. Łazarski, W. Skowroński, J. Kanak, W. Powroźnik, J. Barnaś, F. Stobiecki, T. Stobiecki, Optimization of spin Hall magnetoresistance in heavy-metal/ferromagnetic-metal bilayers, Sci. Rep. 10 (2020) 10767. https://doi.org/10.1038/s41598-020-67450-3.
[35] M.-G. Kang, G. Go, K.-W. Kim, J.-G. Choi, B.-G. Park, and K.-J. Lee. Negative spin Hall magnetoresistance of normal metal/ferromagnet bilayers, Nat. Commun. 11 (2020) 3619. https://doi.org/10.1038/s41467-020-17463-3.
[36] W. Li, Y. Zheng, K. Luo, B. Han, B. Zhang, Y. Guo, J. Cao, Manipulation of spin Hall magnetoresistance and unidirectional spin Hall magnetoresistance in Ta/Pt/CoFeB multilayers, J. Magn. Magn. Mater. 560 (2022) 169667. https://doi.org/10.1016/j.jmmm.2022.169667.
[37] C.-F. Pai, Y. Ou, L.H. Vilela-Leão, D.C. Ralph, R.A. Buhrman. Dependence of the efficiency of spin Hall torque on the transparency of Pt/ferromagnetic layer interfaces, Phys. Rev. B 92 (2015) 064426. https://doi.org/10.1103/PhysRevB.92.064426.
[38] X. Xiao, J.X. Li, Z. Ding, J.H. Liang, L. Sun, Y.Z. Wu, Unusual angular dependent magnetoresistance in single-crystalline Co/Pt bilayers, Appl. Phys. Lett. 108 (2016) 222402. http://dx.doi.org/10.1063/1.4953155.
[39] L. Wang, R.J.H. Wesselink, Y. Liu, Z. Yuan, K. Xia, P.J. Kelly, Giant Room Temperature Interface Spin Hall and Inverse Spin Hall Effects, Phys. Rev. Lett. 116 (2016) 196602. https://doi.org/10.1103/PhysRevLett.116.196602.

[40] W. Zhang, W. Han, X. Jiang, S.-H. Yang, and S.S.P. Parkin, Role of transparency of platinum–ferromagnet interfaces in determining the intrinsic magnitude of the spin Hall effect, Nature Phys. 11 (2015) 496–502. https://doi.org/10.1038/nphys3304.
[41] A. Philippi-Kobs, A. Farhadi, L. Matheis, D. Lott, A. Chuvilin, H.P. Oepen, Impact of Symmetry on Anisotropic Magnetoresistance in Textured Ferromagnetic Thin Films, Phys. Rev. Lett. 123 (2019) 137201. https://doi.org/10.1103/PhysRevLett.123.137201.
[42] Y. Cui, X. Feng, Q. Zhang, H. Zhou, W. Jiang, J. Cao, D. Xue, X. Fan, Absence of spin Hall magnetoresistance in Pt/(CoNi)n multilayers, Phys. Rev. B 103 (2021) 024415. https://doi.org/10.1103/PhysRevB.103.024415.
[43] L.K. Zou, Y. Zhang, L. Gu, J. W. Cai, L. Sun, Tunable angular-dependent magnetoresistance correlations in magnetic films and their implications for spin Hall magnetoresistance analysis, Phys. Rev. B 93 (2016) 075309. https://doi.org/10.1103/PhysRevB.93.075309.
[44] J. Ryu, C.O. Avci, S. Karube, M. Kohda, G.S.D. Beach, J. Nitta, Crystal orientation dependence of spin-orbit torques in Co/Pt bilayers, Appl. Phys. Lett. 114 (2019) 142402. https://doi.org/10.1063/1.5090610.
[45] J. Rodriguez-Carvajal, Recent advances in magnetic structure determination by neutron powder diffraction, Physica B: Cond. Matt. 192 (1993) 55–69. https://doi.org/10.1016/0921-4526(93)90108-i.
[46] N. Soya, H. Hayashi, T. Harumoto, T. Gao, S. Haku, K. Ando, Crossover of the intrinsic spin Hall effect in the presence of lattice expansion, Phys. Rev. B 103 (2021) 174427. https://doi.org/10.1103/PhysRevB.103.174427.
[47] T.N. Anh Nguyen *et al.*, Effect of flattened surface morphology of anodized aluminum oxide templates on the magnetic properties of nanoporous Co/Pt and Co/Pd thin multilayered films, Appl. Surf. Science 427 (2018) 649-655. https://doi.org/10.1016/j.apsusc.2017.08.238.
[48] M. Magnuson, G. Greczynski, F. Eriksson, L. Hultman, H. Högberg, Electronic structure of β-Ta films from X-ray photoelectron spectroscopy and first-principles calculations, Appl. Surf. Science 470 (2019) 607-612. https://doi.org/10.1016/j.apsusc.2018.11.096.
[49] P. He, W.A. McGahan, J.A. Woollam, F. Sequeda, T. McDaniel, H. Do, Magneto-optical Kerr effect and perpendicular magnetic anisotropy of evaporated and sputtered Co/Pt multilayer structures, J. Appl. Phys. 69 (1991) 4021-4026. https://doi.org/10.1063/1.348411.
[50] N. Figueiredo-Prestes, J. Zarpellon, D.S. Costa, I. Mazzaro, P.C. de Camargo, A.J.A. de Oliveira, C. Deranlot, J.-M. George, D.H. Mosca, Thermal Stability of Ultrathin Co/Pt Multilayers, J. Phys. Chem. C 125 (2021) 4885–4892. https://doi.org/10.1021/acs.jpcc.1c00054.
[51] W.-B. Wu *et al.*, Complex magnetic ordering in nanoporous $[Co/Pd]_5$-IrMn multilayers with perpendicular magnetic anisotropy and its impact on magnetization reversal and magnetoresistance, Phys. Chem. Chem. Phys. 22 (2020) 3661-3674. https://doi.org/10.1039/c9cp05947d.
[52] S. Ziętek, J. Mojsiejuk, K. Grochot, S. Łazarski, W. Skowroński, T. Stobiecki, Numerical model of harmonic Hall voltage detection for spintronic devices, Phys. Rev. B 106 (2022) 024403. https://doi.org/10.1103/PhysRevB.106.024403.
[53] T.N. Anh Nguyen *et al.*, Correlation of magnetic and magnetoresistive properties of nanoporous Co/Pd thin multilayers fabricated on anodized TiO2 templates, Sci. Rep. 10 (2020) 10838. https://doi.org/10.1038/s41598-020-67677-0.
[54] W.-B. Wu *et al.*, Influence of interfacial magnetic ordering and field-cooling effect on perpendicular exchange bias and magnetoresistance in nanoporous IrMn/[Co/Pd] films, J. Appl. Phys. 127 (2020) 223904. https://doi.org/10.1063/5.0006194.
[55] J. W. Knepper, F. Y. Yang, Oscillatory interlayer coupling in Co/Pt multilayers with perpendicular anisotropy, Phys. Rev. B 71 (2005) 224403. https://doi.org/10.1103/PhysRevB.71.224403.

[56] S.Y. Huang, X. Fan, D. Qu, Y.P. Chen, W.G. Wang, J. Wu, T.Y. Chen, J.Q. Xiao, C.L. Chien, Transport Magnetic Proximity Effects in Platinum, Phys. Rev. Lett. 109 (2012) 107204. https://doi.org/10.1103/PhysRevLett.109.107204.
[57] W. Zhang, M.B. Jungfleisch, W. Jiang, Y. Liu, J.E. Pearson, S.G.E. Velthuis, A. Hoffmann, Reduced spin-Hall effects from magnetic proximity, Phys. Rev. B 91 (2015) 115316. https://doi.org/10.1103/PhysRevB.91.115316.
[58] C.O. Avci, K. Garello, A. Ghosh, M. Gabureac, S.F. Alvarado, P. Gambardella, Unidirectional spin Hall magnetoresistance in ferromagnet/normal metal bilayers, Nature Phys. 11 (2015) 570–575. https://doi.org/10.1038/nphys3356.
[59] H.B. Vasili, M. Gamino, J. Gàzquez, F. Sánchez, M. Valvidares, P. Gargiani, E. Pellegrin, J. Fontcuberta, Magnetoresistance in Hybrid Pt/CoFe2O4 Bilayers Controlled by Competing Spin Accumulation and Interfacial Chemical Reconstruction, ACS Appl. Mater. Interfaces 10 (2018) 12031−12041. https://doi.org/10.1021/acsami.8b00384.
[60] W. Gil, D. Görlitz, M. Horisberger, and J. Kötzler, Magnetoresistance anisotropy of polycrystalline cobalt films: Geometrical-size and domain effects, Phys. Rev. B 72 (2005) 134401. https://doi.org/10.1103/PhysRevB.72.134401.
[61] X. Huang, Z. Dai, L. Huang, G. Lu, M. Liu, H. Piao, D-H Kim, S. Yu, L. Pan, Spin Hall magnetoresistance in Co_2FeSi/Pt thin films: dependence on Pt thickness and temperature, J. Phys.: Condens. Matter. 28 (2016) 476006. http://dx.doi.org/10.1088/0953-8984/28/47/476006.
[62] T. Lin, C. Tang, H.M. Alyahayaei, J. Shi, Experimental Investigation of the Nature of the Magnetoresistance Effects in Pd-YIG Hybrid Structures, Phys. Rev. Lett. 113 (2014) 037203. https://doi.org/10.1103/PhysRevLett.113.037203.
[63] S.R. Marmion, M. Ali, M. McLaren, D.A. Williams, B.J. Hickey, Temperature dependence of spin Hall magnetoresistance in thin YIG/Pt films, Phys. Rev. B 89 (2014) 220404(R). https://doi.org/10.1103/PhysRevB.89.220404.
[64] C.O. Avci, K. Garello, J. Mendil, A. Ghosh, N. Blasakis, M. Gabureac, M. Trassin, M. Fiebig, P. Gambardella, Magnetoresistance of heavy and light metal/ferromagnet bilayers, Appl. Phys. Lett. 107 (2015) 192405. https://doi.org/10.1063/1.4935497.
[65] C.O. Avci, K. Garello, M. Gabureac, A. Ghosh, A. Fuhrer, S.F. Alvarado, P. Gambardella, Interplay of spin-orbit torque and thermoelectric effects in ferromagnet/normal-metal bilayers, Phys. Rev. B 90 (2014) 224427. https://doi.org/10.1103/PhysRevB.90.224427.
[66] K. Zhang, L. Chen, Y. Zhang, B. Hong, Y. He, K. Lin, Z. Zhang, Z. Zheng, X. Feng, Y. Zhang, Y. Otani, W. Zhao, Efficient and controllable magnetization switching induced by intermixing-enhanced bulk spin–orbit torque in ferromagnetic multilayers, Appl. Phys. Rev. 9 (2022) 011407. https://doi.org/10.1063/5.0067348.
[67] V.P. Amin, M.D. Stiles, Spin transport at interfaces with spin-orbit coupling: Formalism, Phys. Rev. B 94 (2016) 104419. https://doi.org/10.1103/PhysRevB.94.104419.
[68] V.P. Amin, M.D. Stiles, Spin transport at interfaces with spin-orbit coupling: Phenomenology, Phys. Rev. B 94 (2016) 104420. https://doi.org/10.1103/PhysRevB.94.104420g/10.1103/PhysRevB.90.224427.

Figure captions

Figure 1. A scheme of electrical probes arrangement and definition of polar and azimuthal angles setting the orientation of magnetization $M(\theta, \varphi)$ and external magnetic field $B(\theta_B, \varphi_B)$ in spherical coordinates

Figure 2. (a-b) XRD patterns of Pt/[Co/Pt] film with 15 nm (a) and 3 nm (b) thick Pt underlayer accompanied by their approximation and phase decomposition; (c) HRTEM image of Pt/[Co/Pt] film with 15 nm thick Pt underlayer; (d) enlarged images of selected areas of [Co/Pt] MLs obtained by HRTEM (upper panel) and processed according to FFT procedure (lower panel); (e) inverse FFT images obtained from the regions of Pt underlayer and [Co/Pt] MLs; red dots in (e) correspond to the calculated atoms positions for Pt (a = 3.897 Å) and CoPt (a = 3.840 Å) *fcc* lattices.

Figure 3. (a)-(c) Field dependences of normalized magnetization obtained at different temperatures T = 3-300 K: (a) m_z projection in B_z field; (b) m_z projection in B_y field; (c) m_y projection in B_y field; (d) field dependences of magnetization orientation $\theta(B_y)$ at T = 3-300 K; (e) temperature dependences of coercive field $B_C(T)$ in B_z field (red line) and switching field $B_R(T)$ in B_y field (black scatters and shaded area limited by the curves corresponding to the beginning and completion of the magnetization reversal transition); (f) field dependences of in-plane magnetization $M_y(B_y)$ (in the absolute values of net magnetic moment); (g) temperature dependence of saturation magnetization (net magnetic moment) $M_S(T)$.

Figure 4. (a) Angular dependences of normalized longitudinal resistance $\Delta R(\theta_B)/\Delta R_{max}$; (b) the corresponding angular dependences of AHE voltage $U_{AHE}(\theta_B)$ and (c) magnetization orientation $\theta(\theta_B)$ on the direction of magnetic field θ_B rotating in zy plane (B = 4 T); (d) approximation of $R(\theta_B)$ dependences and their decomposition into ~$\sin^2\theta$ and ~$\cos^4\theta$ components; right axis in (d) show the corresponding MR ratios.

Figure 5. (a)-(c) Field dependences of resistance $R(B)$ measured at T = 200 K (a) and T = 10 K (b), (c) in B_z and B_y magnetic field; the inset in (b) shows the corresponding angular $R(\theta_B)$ dependence; the $R(B_y)$ curve in (c) is decomposed into ~$\sin^2\theta$, ~$\cos^4\theta$ and Lorentz contributions; (d) field dependences of MR ratios obtained at different temperatures T = 3–300 K in B_y magnetic field; (e) field dependences of AMR effect obtained at different temperatures T = 3–250 K in B_x magnetic field; (f) temperature dependences of the amplitude of the AMR effect

obtained in B_x and B_y magnetic field accompanied by temperature dependence of saturation magnetization (net magnetic moment) $M_S(T)$.

Figure 6. (a) Field dependences of the first $U_H^f(B_y)$ and second $U_H^{2f}(B_y)$ harmonic Hall voltage obtained at T = 10 K in the field B sweeping in θ_B = 85° direction; red solid line shows $U_H^{2f}(B_y)$ curve modeled using Eq. (4); (b) effective field $B_{FL}/\cos\theta$ obtained according to Eq. (5) as a function of external field B_y; the inset show the $B_{FL}(\theta)$ dependence derived; (c)-(h) angular dependences (zy scans) of the second harmonic Hall voltage $U_H^{2f}(\theta_B)$ obtained at T = 10 K (c), (e), (f); T = 100 K (d), (g); and T = 250 K (h) in the fixed external field B = 4 T (green scatter) and B = 2 T (orange scatters). The solid lines in (c) and (d) show $\cos(k\cdot\theta_B)$ function scaled from the experimental curves, while the dotted lines in (e)-(h) show approximations by the function $\sim dU^f_H/d\theta_B \cdot \cos(l\cdot\theta)$ according to Eq. (3).

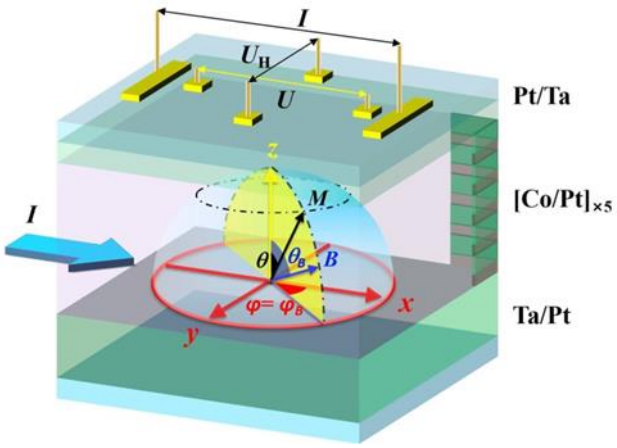

Figure1

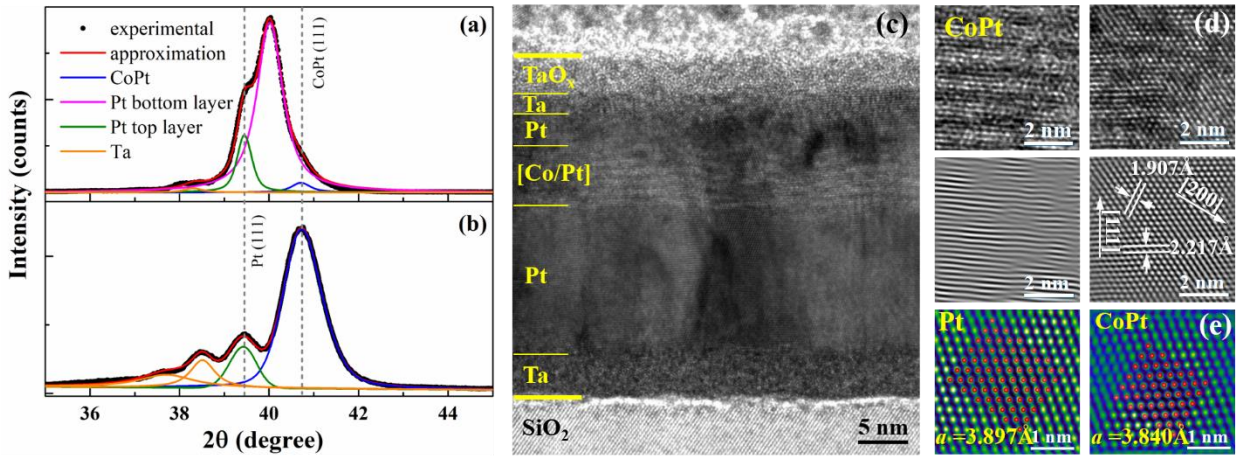
(a)
experimental
approximation
CoPt
Pt bottom layer
Pt top layer
Ta
CoPt (111)
(b)
Pt (111)
Intensity (counts)
36
38
40
42
44
2θ (degree)
(c)
TaO
Ta
Pt
[Co/Pt]
Pt
Ta
SiO2
5 nm
CoPt
2 nm
(d)
2 nm
2 nm
1.907Å
(200)
(111)
2.217Å
2 nm
Pt
a =3.897Å
1 nm
CoPt
(e)
a =3.840Å
1 nm

Figure 2

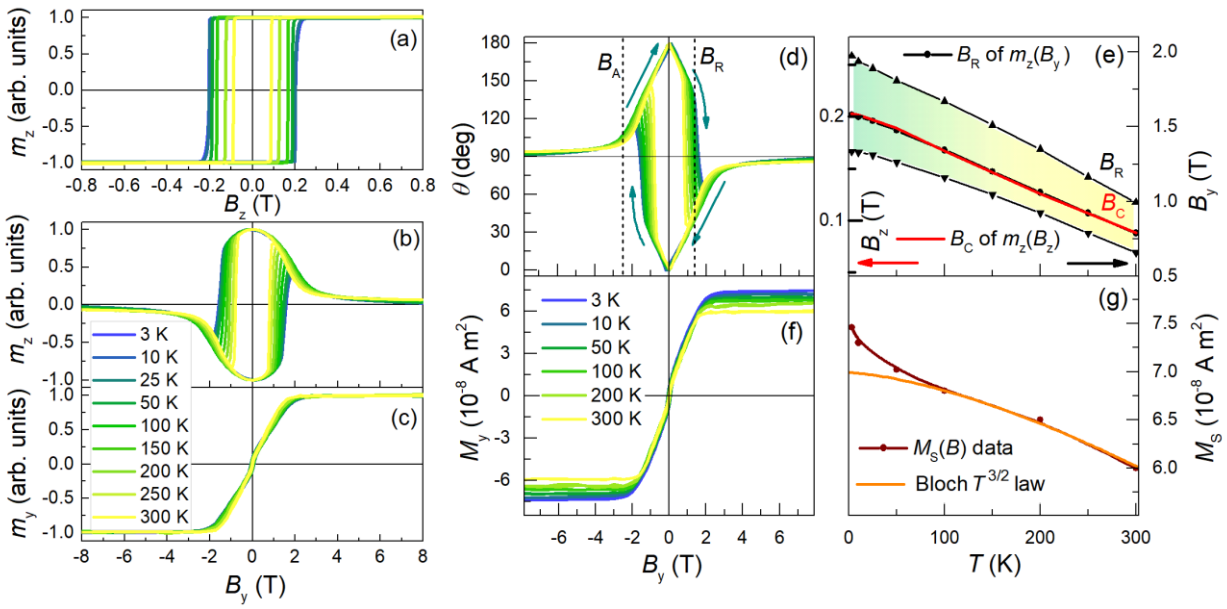
(a)
(b)
(c)
(d)
(e)
(f)
(g)
m_z (arb. units)
m_y (arb. units)
B_z (T)
B_y (T)
3 K
10 K
25 K
50 K
100 K
150 K
200 K
250 K
300 K
θ (deg)
B_A
B_R
M_y (10^{-8} A m^2)
B_R of $m_z(B_y)$
B_C of $m_z(B_z)$
B_C
M_S (10^{-8} A m^2)
$M_S(B)$ data
Bloch $T^{3/2}$ law
T (K)

Figure 3

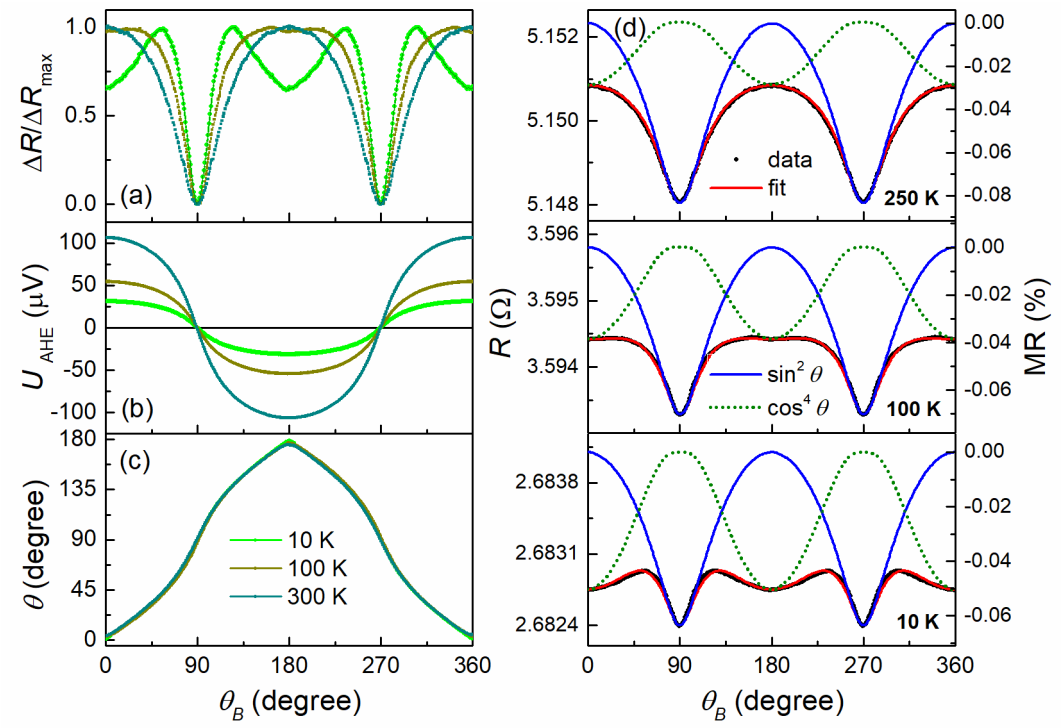
(a)
(b)
(c)
(d)
$\Delta R/\Delta R_{max}$
U_{AHE} (μV)
θ (degree)
R (Ω)
MR (%)
θ_B (degree)
10 K
100 K
300 K
data
fit
250 K
100 K
10 K
$\sin^2\theta$
$\cos^4\theta$

Figure 4

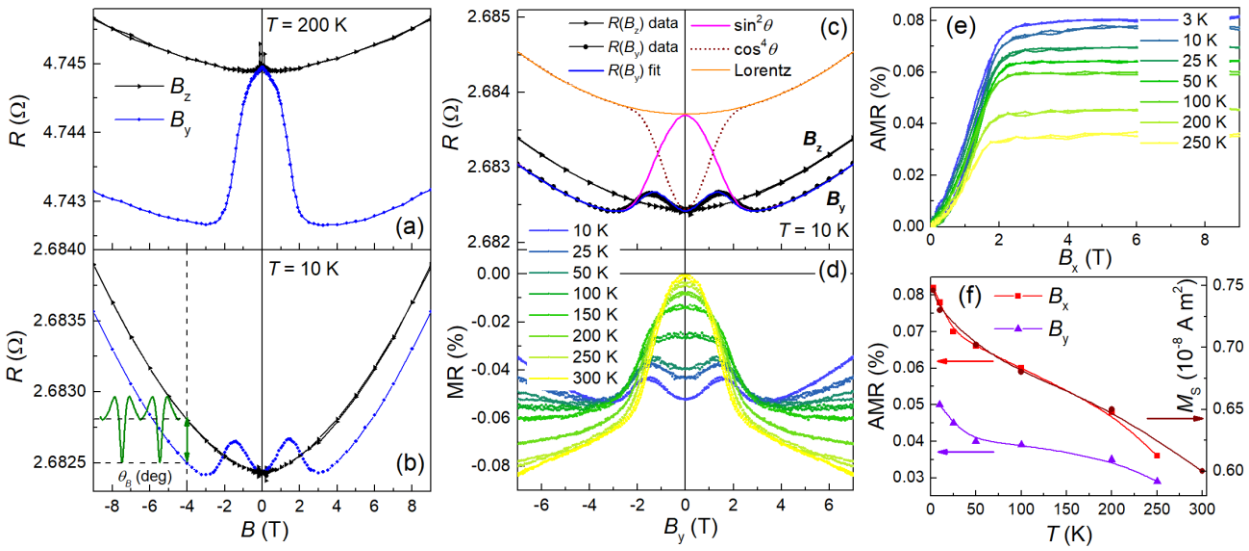
T = 200 K
B_z
B_y
(a)
R (Ω)
T = 10 K
(b)
θ_B (deg)
B (T)
R(B_z) data
R(B_y) data
R(B_y) fit
sin²θ
cos⁴θ
Lorentz
(c)
B_z
B_y
T = 10 K
10 K
25 K
50 K
100 K
150 K
200 K
250 K
300 K
(d)
MR (%)
B_y (T)
(e)
AMR (%)
3 K
10 K
25 K
50 K
100 K
200 K
250 K
B_x (T)
(f)
B_x
B_y
M_S (10⁻⁸ A m²)
T (K)

Figure 5

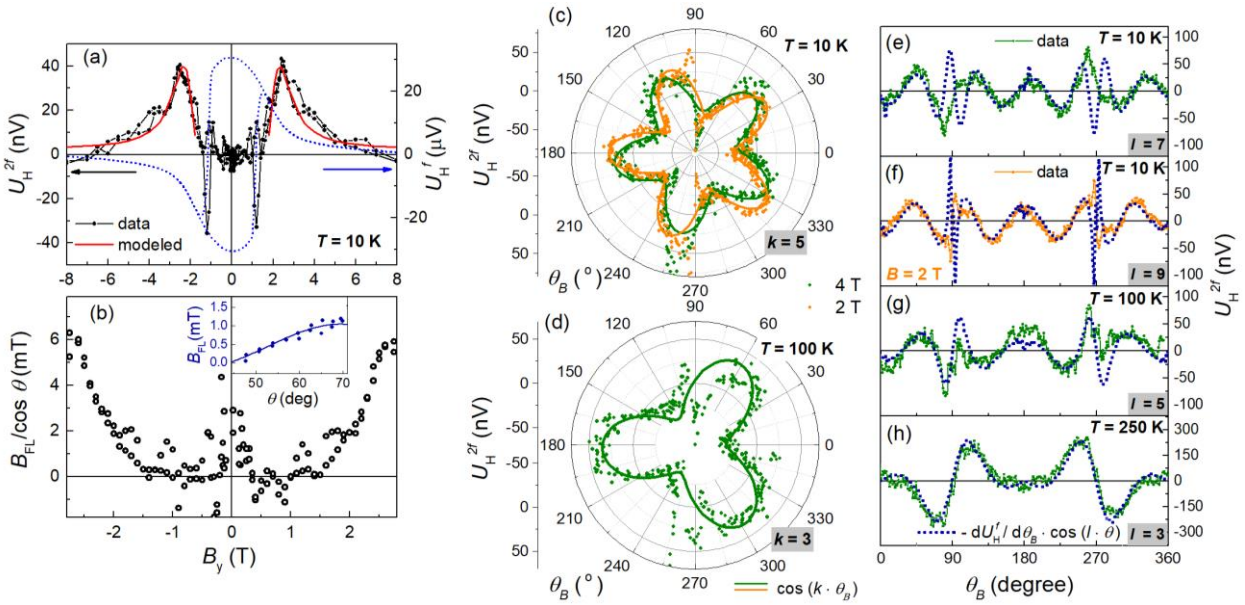
(a)
data
modeled
T = 10 K
(b)
(c)
T = 10 K
k = 5
4 T
2 T
(d)
T = 100 K
k = 3
cos (k · θB)
(e)
data
T = 10 K
l = 7
(f)
data
T = 10 K
B = 2 T
l = 9
(g)
T = 100 K
l = 5
(h)
T = 250 K
l = 3
θB (degree)

Figure 6